PARAMETRIC STUDY OF THE EXPANSIVE JOINT MODEL FOR CRACKING OF CONCRETE DUE TO REBAR CORROSION

B. Sanz[1*], J. Planas[1], J.M. Sancho[2]

[1]Dep. de Ciencia de Materiales, E.T.S. de Ingenieros de Caminos, Canales y Puertos, Universidad Politécnica de Madrid, C/ Profesor Aranguren s/n, 28040 Madrid, España.
E-mail: bsanz@mater.upm.es
E-mail: jaime.planas@upm.es

[2]Dep. de Estructuras de Edificación, E.T.S. de Arquitectura, Universidad Politécnica de Madrid, Avda. Juan de Herrera 4, 28040 Madrid, España.
E-mail: jose.sancho@upm.es

[*]Corresponding author

ABSTRACT

A numerical model called *expansive joint element* was programmed to simulate the mechanical expansion of the oxide and to study the cracking on the surrounding concrete. The expansive joint element works together with finite elements with embedded adaptable cohesive crack to simulate the fracture of concrete according to the cohesive crack model. That model was proved to properly reproduce the crack pattern observed in samples of reinforced concrete with accelerated corrosion. In this work, a parametric study of the expansive joint element is carried out to establish the computational limits of the constitutive parameters of the oxide. A certain expansion is simulated varying the oxide parameters and the crack opening width and the stresses in concrete that are obtained during the process are analyzed. The range of values for which the results of the simulations are nearly identical, with the minimum number of iterations, are determined.

RESUMEN

Un modelo numérico llamado *elemento junta expansiva* fue programado para simular la expansión mecánica del óxido y estudiar la fisuración en el hormigón circundante. El elemento junta expansiva trabaja con elementos finitos con fisura cohesiva embebida adaptable para simular la fractura del hormigón según el modelo de fisura cohesiva. Se ha comprobado que el modelo reproduce correctamente el patrón de fisuración del hormigón que se obtiene en ensayos de corrosión acelerada. En este trabajo, se realiza un estudio paramétrico del elemento junta expansiva para establecer los límites de los parámetros constitutivos del óxido. Se simula una cierta expansión variando los valores de los parámetros del óxido y se estudian la apertura de fisura y las tensiones resultantes en el hormigón. Se determina el rango de valores para los que los resultados de las simulaciones son prácticamente iguales, con el menor número posible de iteraciones.

KEY WORDS: Corrosion, Cohesive crack, Finite Elements simulations

1 INTRODUCTION

One of the effects of corrosion of rebars in reinforced concrete structures is the volumetric expansion of the oxide layer, which produces the cracking of the surrounding concrete [1, 2, 3]. To study and simulate such an effect, a numerical model, already presented in previous conferences, was programmed [4].

In that model, finite elements with embedded adaptable cohesive crack [5] that follow the cohesive crack model proposed by Hillerborg [6] are used to simulate fracture of concrete. To simulate the volumetric expansion and the mechanical behavior of the oxide, a finite element so called *expansive joint element* was programmed within the finite element framework COFE (*Continuum Oriented Finite Element*).

The crack pattern predicted by the simulations was found to properly reproduce the crack pattern observed in real samples with accelerated corrosion [7]. In that study, the geometry of the cross-section in the tests was simulated and the mechanical and fracture properties of concrete were experimentally determined by compression, brazilian and three point bending tests [8, 9, 10, 11, 12]. However, no experimental results are available for the parameters of the oxide; thus, their values had to be estimated so as to keep the calculations stable.

In this work, the numerical limits of the main parameters of the model are established. The constitutive parameters of the oxide are varied to find the range of values for which the curves of crack opening width and compressive stress in concrete overlap, while keeping the calculations stable.

2 BASIS OF THE EXPANSIVE JOINT ELEMENT

The expansive joint element was programmed to reproduce the mechanical expansion of the oxide at the steel surface when the steel bars of a reinforced concrete structure are corroding.

The element consists in a four-node element with zero initial thickness that is defined by its initial length and the normal direction to its faces. The model works assuming elastic behavior, small strain and direct integration at the nodes. It is implemented within the finite element framework COFE (*Continuum Oriented Finite Elements*), which is a particular finite element program with strong discontinuity kinematics, constant strain elements, central force cohesive model and limited crack adaptation as its main features.

Two main parameters of the model are the corrosion depth x, which is the amount of sound steel that is transformed into oxide, and the expansion factor β. The volumetric expansion of the oxide, which is produced due to the greater specific volume of the oxide respect to the steel, has a value equal to βx, as shown in figure 1.

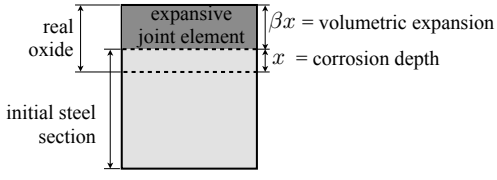

Figure 1: Sketch of the expansive joint element.

In the expansive joint element, only the volumetric expansion is considered as oxide, and the steel section is kept invariable, to avoid re-meshing during the calculations. Thus, mechanical equivalence has to be established between the real and the simulated sections, so that identical displacements are obtained when a certain traction vector is applied to the real and to the simulated oxide. Then, as shown in [4], it turns out that the normal and shear stiffness k_n and k_t of the expansive joint element are inversely proportional to the corrosion depth x:

$$k_n = \frac{K_n}{\beta x} \qquad \text{and} \qquad k_t = \frac{K_t}{\beta x} \tag{1}$$

where the normal and tangential moduli of the expansive joint element K_n and K_t are directly related to the properties of the steel and the real oxide. Since for $x \to 0$, k_n and $k_t \to \infty$ and the system becomes numerically unstable, a cut-off is established. Then, the normal stiffness is calculated as follows:

$$k_n = \begin{cases} k_n^0 & x \le x_0 \\ k_n^0 \dfrac{x_0}{x} & x > x_0 \end{cases} \tag{2}$$

where k_n^0 and x_0 are the cut-offs of the normal stiffness and the corrosion depth, and a similar expression is obtained for the shear stiffness, with a cut-off k_t^0.

Finally, a directionality factor η_t is introduced in the formulation of the element to reduce the normal stiffness in the case of tension stress in the element. Then, the normal stiffness k_n that is shown in equation (2) is multiplied by the directionality factor η_t, which has the following values:

$$\eta_t = \begin{cases} 1 & \text{in the case of compression} \\ \ll 1 & \text{in the case of tension} \end{cases} \tag{3}$$

3 PARAMETRIC STUDY

3.1 Geometry and materials

The samples in the simulations are concrete prisms of 100 mm width and 90 mm height with a 20 mm diameter steel bar that is centered respect to the width and with a cover equal to the diameter of the bar.

The mesh is generated using the pre-post FE mesh processor Gmsh [13] and the elements of steel and concrete are constant strain triangles.

The concrete is modeled with elements with embedded adaptable cohesive crack [5], the steel with linear elastic material and the oxide with expansive joint elements.

The mechanical properties of the steel have been adopted according to standard values of this material. The fracture properties of the concrete have been determined with compression, brazilian and three point bending tests [9, 11] and an inverse analysis has been carried out to obtain the main parameters of the softening curve [8, 10, 12]. In the simulations, the softening curve of concrete has been modeled with a linear softening curve, which contains half of the total fracture energy of the actual softening curve of concrete. The values of all the parameters are shown in table 1.

Table 1: Mechanical properties of steel and concrete, where E is the elasticity modulus, ν is the Poisson coefficient, α' is the adaption factor of the crack, f_t is the tensile strength and G_F is the fracture energy.

	Steel	Concrete
E (GPa)	200	30
ν	0.3	0.2
α'	–	0.2
f_t (MPa)	–	3.0
G_F (N/mm)	–	0.05

For the stiffness of the oxide, no experimental values are available, so they have to be assumed 'a priori'. For the expansion factor β, a value equal to one was found in the literature [1, 2] and it has been adopted in the calculations.

3.2 Parameters of this study and reference values

For the parameters of the expansive joint element, some values were initially estimated according to the following: first, the oxide was assumed to behave as water [2], thus, the bulk modulus K_n of the expansive joint element was calculated in relation to the moduli of steel and water and, from that, the initial normal stiffness k_n^0 of the element was calculated; second, a previous study with the element [4] revealed that very small shear stiffness k_t and strongly reduced stiffness in tension, which is obtained with a very small value of the directionality factor η_t, have to be assumed to get proper localization of the cracks and to relieve concentration of stresses at the steel,

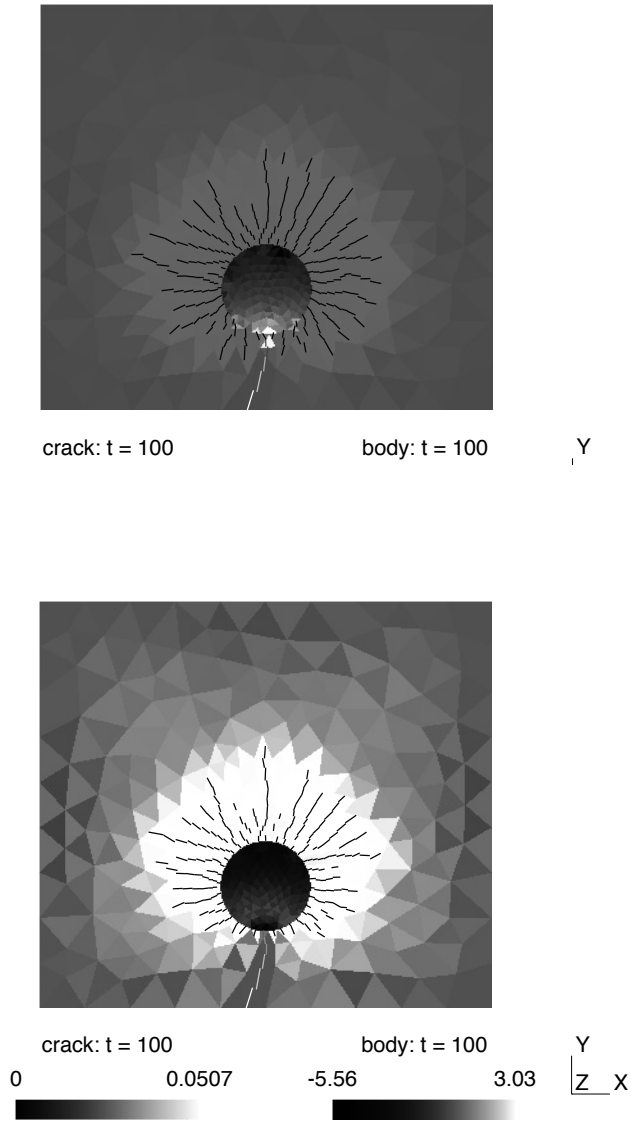

Figure 2: Stress distribution in a concrete section without reducing the normal stiffness of the oxide (up) and with strongly reduced normal stiffness in tension (bottom).

The cut-off corrosion depth x_0, the size of the mesh, given by the number of elements along the circumference of the rebar, the step size in corrosion depth and the tolerance were also arbitrarily chosen.

In the present work, the limits for which there is little or no influence on the results with the best convergence are studied for the constitutive parameters of the oxide. The values that were initially chosen have been adopted as reference in this study, they are kept constant while looking for the limits of each parameter, and are shown in table 2.

Table 2: Reference values for this study, where k_n^0 is the cut-off normal stiffness in compression, k_t^0 is the cut-off shear stiffness, x_0 is the cut-off corrosion depth, η_t is the directionality factor to reduce the normal stiffness in tension and n is the number of elements per quarter of the rebar circumference.

parameter	reference value
k_n^0 (N/mm^3)	$7.0 \cdot 10^6$
k_t^0 (N/mm^3)	$7.0 \cdot 10^{-14}$
x_0 (mm)	$1.0 \cdot 10^{-3}$
η_t	$1.0 \cdot 10^{-11}$
n	8
step (μm)	0.5
tol	$1.0 \cdot 10^{-6}$

The range of validity of each parameter is determined by looking for the values for which the curves of maximum crack opening width and maximum compressive stress overlap, while keeping the number of iterations as low as possible.

4 RESULTS

4.1 Limits of the normal stiffness in compression k_n^0

For corrosion depths greater than the cut-off x_0, the normal stiffness of the expansive joint element k_n depends on the product $K_n = k_n^0 x_0$, as shown in equation (2). In this study, the influence of the cut-off normal stiffness k_n^0 is analyzed keeping constant the parameter x_0, so the curves of stiffness are as shown in figure 3.

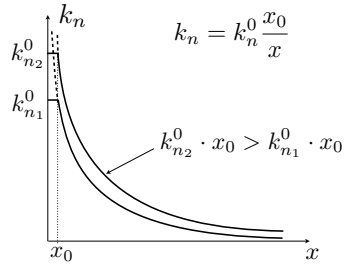

Figure 3: Sketch of the curves of normal stiffness when k_n^0 is varied but x_0 is kept constant.

From the analysis of the curves of maximum crack opening width versus corrosion depth, it is found that the curves are basically identical for values within the range $7 \cdot 10^5 \leq k_n^0 \leq 7 \cdot 10^9$ N/mm^3, as seen in figure 4.

When the curves of maximum compressive stress are compared, however, the range for which the curves overlap is restricted to $7 \cdot 10^6 \leq k_n^0 \leq 7 \cdot 10^8$ N/mm^3, as shown in figure 5.

Finally, it is found that for values of $k_n^0 \geq 7 \cdot 10^6$ N/mm^3, the number of iterations systematically increases with k_n^0, as shown in figure 6. Therefore, k_n^0 should be kept as low as possible within the previously established ranges and, thus, the optimal cut-off normal stiffness (from a strictly numerical point of view) is: $k_n^0 = 7 \cdot 10^6$ N/mm^3.

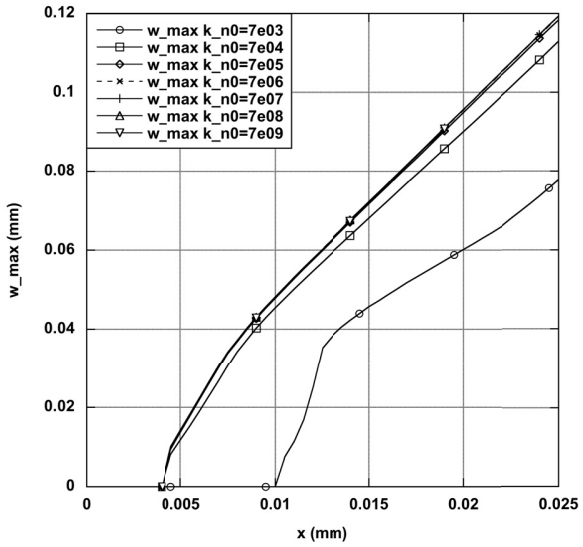

Figure 4: Influence of the normal stiffness k_n^0 on the curves of maximum crack width versus corrosion depth.

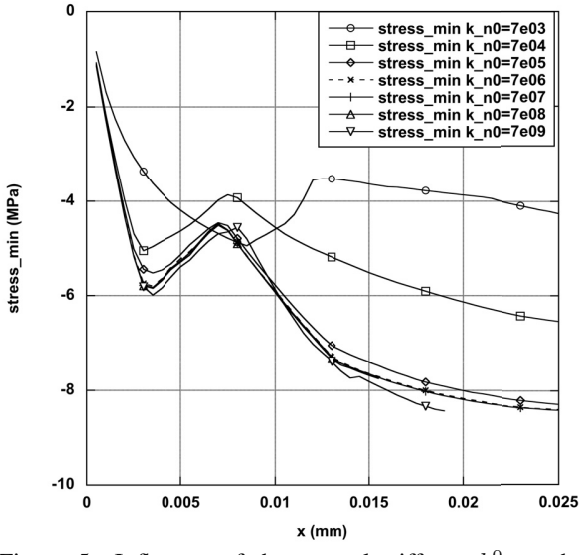

Figure 5: Influence of the normal stiffness k_n^0 on the curves of maximum compressive stress versus corrosion depth.

That optimum value and the fixed cut-off corrosion depth x_0 define an optimum curve k_n for the normal stiffness with constant $K_n = k_n^0 x_0 = 7 \cdot 10^3$ MPa.

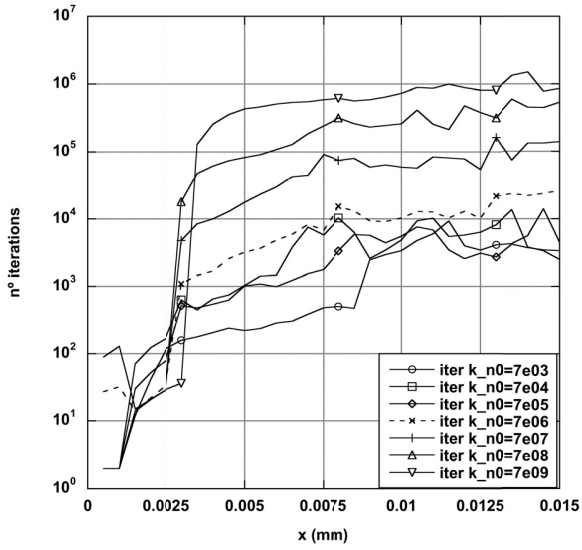

Figure 6: Influence of the normal stiffness k_n^0 on the curves of number of iterations versus corrosion depth.

4.2 Limits of the shear stiffness k_t^0

As in the previous case, the curves of maximum crack width and maximum compressive stress versus corrosion depth are studied to determine the range for the cut-off shear stiffness k_t^0.

First, figure 7 shows that the curves of maximum crack opening versus corrosion depth overlap for $k_t^0 \leq 70$ N/mm^3.

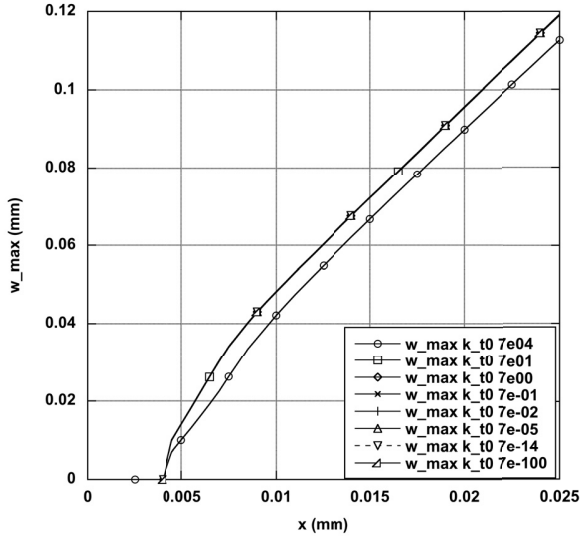

Figure 7: Influence of the shear stiffness k_t^0 on the curves of maximum crack width versus corrosion depth.

Next, the curves of maximum compressive stress narrow the range to $k_t^0 \leq 7$ N/mm^3, as shown in figure 8.

The curves of number of iterations versus corrosion depth are almost identical for $k_t^0 \leq 70$ N/mm^3, as shown in figure 9, so not additional information is provided. Then, the valid range of values for the cut-off shear stiffness k_t^0 is the range determined by the compression curves: $k_t^0 \leq 7$ N/mm^3.

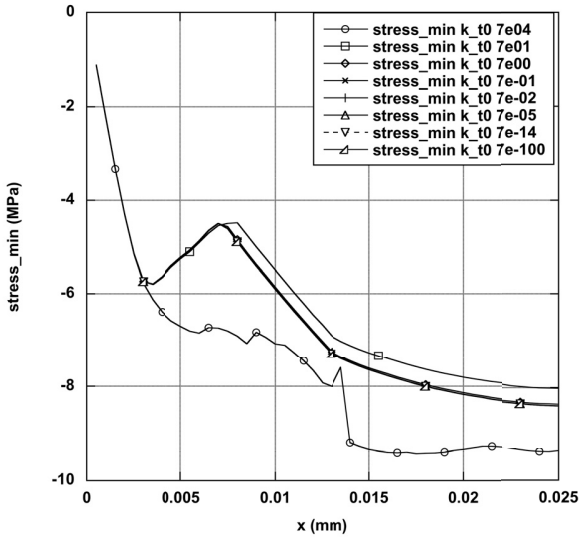

Figure 8: Influence of the shear stiffness k_t^0 on the curves of maximum compressive stress versus corrosion depth.

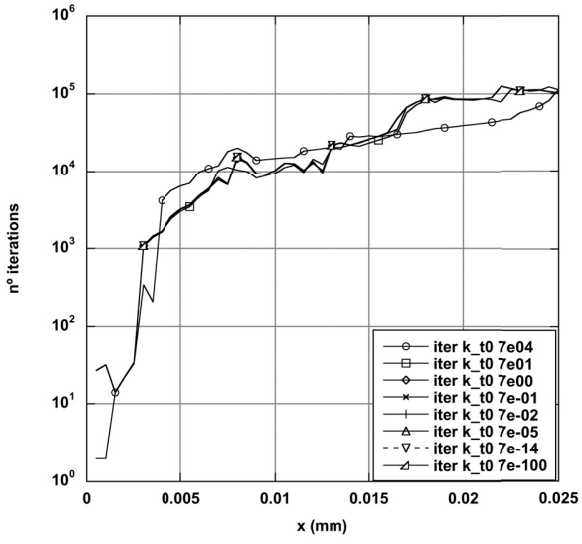

Figure 9: Influence of the shear stiffness k_t^0 on the curves of number of iterations versus corrosion depth.

4.3 Limits of the directionality factor η_t

To determine the limits of the directionality factor η_t, which reduces the normal stiffness in tension, the maximum crack opening, the maximum compressive stress and the number of iterations are studied.

From the curves of maximum crack opening, an initial valid range $\eta_t \leq 1 \cdot 10^{-4}$ is established, as shown in figure 10.

The curves of maximum compressive stress restrict the latter range to $\eta_t \leq 1 \cdot 10^{-5}$, as seen in figure 11.

For $\eta_t \leq 1 \cdot 10^{-5}$, the curves of number of iterations overlap, as shown in figure 12, and, thus, not additional information is obtained from those curves. Then, the valid range of values for the directionality factor η_t is determined by the compression curves and equal to $\eta_t \leq 1 \cdot 10^{-5}$, equivalent to an upper bound for the normal stiffness in tension of 70 N/mm^3.

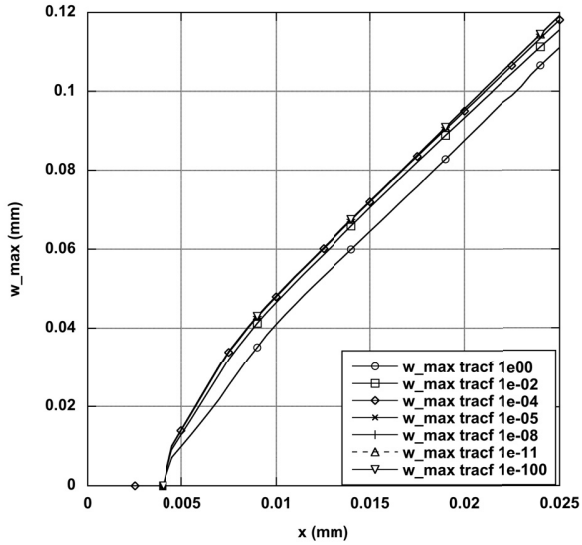

Figure 10: Influence of the directionality factor η_t on the curves of maximum crack width versus corrosion depth.

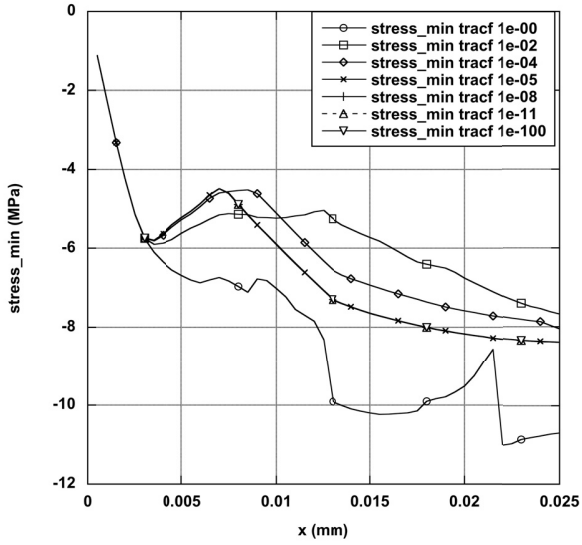

Figure 11: Influence of the directionality factor η_t on the curves of maximum compressive stress versus corrosion depth.

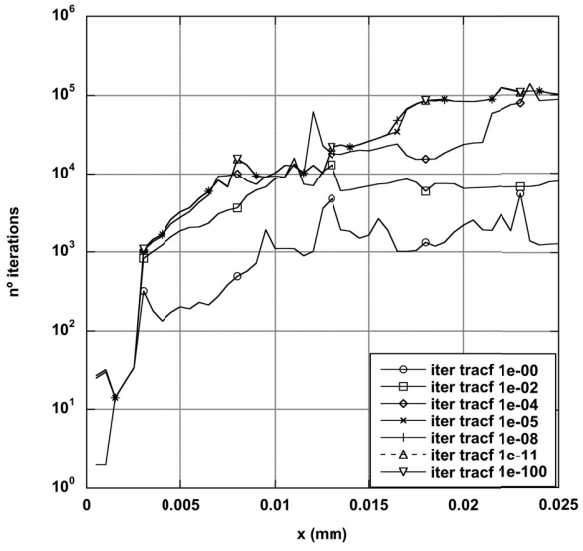

Figure 12: Influence of the directionality factor η_t on the curves of number of iterations versus corrosion depth.

5 CONCLUSIONS

A parametric study of the expansive joint element has been carried out to find the numerical limits of the constitutive parameters of the oxide model.

An optimum value of the cut-off normal stiffness k_n^0 within the range leading to overlapping curves of maximum crack width and maximum compressive stress in concrete has been found as the one giving the lowest number of iterations.

For the shear stiffness k_t^0 and for the directionality factor η_t, which is used to reduce the normal stiffness in tension, there is a range of values for which the results are nearly identical and the convergence is stable.

ACKNOWLEDGEMENTS

The authors gratefully acknowledge the *Ministerio de Ciencia e Innovación, Spain,* for providing financial support for this work under grant BIA2005-09250-C03-01, and for providing, within the Spanish National Research Program CONSOLIDER-INGENIO 2010, funds for the research framework SEDUREC, within which the authors carried out their work.

REFERENCES

[1] C. Andrade, M.C. Alonso, and F.J. Molina. Cover cracking as a function of bar corrosion: Part i - experimental test. *Materials and Structures*, 26:453–464, 1993.

[2] F.J. Molina, M.C. Alonso, and C. Andrade. Cover cracking as a function of bar corrosion: Part ii - numerical model. *Materials and Structures*, 26:532–548, 1993.

[3] M.C. Alonso, C. Andrade, J. Rodriguez, and J.M. Diez. Factors controlling cracking of concrete affected by reinforcement corrosion. *Materials and Structures*, 31:435–441, 1997.

[4] B. Sanz, J. Planas, A. M. Fathy, and J. M. Sancho. Modelización con elementos finitos de la fisuración en el hormigón causada por la corrosión de las armaduras. *Anales de Mecánica de la Fractura*, 25:623–628, 2008.

[5] J. M. Sancho, J. Planas, D. A. Cendon, E. Reyes, and J. C. Galvez. An embedded cohesive crack model for finite element analysis of concrete fracture. *Engineering Fracture Mechanics*, 74:75–86, 2007.

[6] A. Hillerborg, M. Modéer, and P.E. Petersson. Analysis of crack formation and crack growth in concrete by means of fracture mechanics and fracture elements. *Cement and concrete research*, 6:773–782, 1976.

[7] B. Sanz, J. Planas, and J.M. Sancho. Comparison of the crack pattern in accelerated corrosion tests and in finite elements simulations. *Anales de la Mecánica de Fractura*, 2010.

[8] G. V. Guinea, J. Planas, and M. Elices. A general bilinear fitting for the softening curve of concrete. *Materials and Structures*, 27:99–105, 1994.

[9] M. Elices, G. V. Guinea, and J. Planas. On the measurement of concrete fracture energy using three point bend tests. *Materials and Structures*, 30:375–376, 1997.

[10] Z.P. Bazant and J. Planas. *Fracture and size effect in concrete and other quasibrittle materials*. C.R.C. Press, Boca Raton, F.L., 1998.

[11] J. Planas, G. V. Guinea, J. C. Galvez, B. Sanz, and A. M. Fathy. Experimental determination of the stress-crack opening curve for concrete in tension. report 39. chapter 3. indirect tests for stress-crack opening curve. Technical report, RILEM TC 187-SOC Final Report, 2007.

[12] Adel M. Fathy, Beatriz Sanz, J. M. Sancho, and Jaime Planas. Determination of the bilinear stress-crack opening curve for normal- and high-strength concrete. *Fatigue and Fracture of Engineering Materials and Structures*, 31:539–548, 2008.

[13] C. Geuzaine and J.-F. Remacle. Gmsh: a three-dimensional finite element mesh generator with built-in pre- and post-processing facilities. *International Journal for Numerical Methods in Engineering*, 79(11):1309–1331, 2009.